Int J Adv Manuf Technol (2016) 87:399–409
DOI 10.1007/s00170-016-8482-y

ORIGINAL ARTICLE

Finite element analysis of surface milling of carbon fiber-reinforced composites

Seyedbehzad Ghafarizadeh[1] · **Jean-François Chatelain**[1] · **Gilbert Lebrun**[2]

Received: 5 November 2015 / Accepted: 1 February 2016 / Published online: 22 February 2016

Abstract Despite increased applications of carbon fiber-reinforced plastic (CFRP) materials in many industries, such as aerospace, their machining is still a challenge due to their heterogeneity and anisotropic nature. In this research, a finite element model is used to investigate the cutting forces, chip formation mechanism, and machining damage present during the flat end milling of unidirectional CFRP. The material is modeled as an equivalent orthotropic homogeneous material, and Hashin's theory is used to characterize failure in plane stress conditions. The friction coefficient between the tool and the composite material was assumed to be dependent on the carbon fiber orientation. A comparison of modeling and experimental results indicates that the model successfully predicts the cutting forces. The numerical model predictions of machining damage around the cutting area due to fiber compression damage and matrix cracking and the relation between damage extension and fiber orientation are confirmed through a comparison with SEM images of machined edges and surfaces.

Keywords Carbon fiber-reinforced plastics · Milling · Finite element analysis · Machining damage · Cutting forces

✉ Jean-François Chatelain
Jean-Francois.Chatelain@etsmtl.ca

[1] École de technologie supérieure, Université du Québec, Montreal, Canada

[2] Université du Québec à Trois-Rivières (UQTR), Trois-Rivières, Canada

1 Introduction

Carbon fiber-reinforced plastics offer high strength and stiffness-to-weight ratio, low density, long fatigue life, and high corrosion and wear resistances, which make them one of the most important composite materials used in many industries, such as aerospace, construction, and transportation, as well as for medical and military applications.

Carbon fiber-reinforced plastic (CFRP) parts are usually produced to near net-shape, but some machining operations, such as milling, drilling, and trimming, are often required to remove excess materials and bring the parts to the final size and shape [1]. The machining of CFRP materials is a challenging process, due to their heterogeneity and anisotropic behavior, and can generate some damages, such as fiber fragmentation, fiber pullout, matrix softening/melting, matrix cracking, fuzzing, burring, and delamination.

Experimental research on composite machining is not only expensive and time-consuming, but also the carbon chips that are produced during machining of CFRP are dangerous for human health. In addition, interpreting the experimental results is difficult due to the complexity of the milling process and the anisotropy of the composites [2]. In recent years, therefore, with the improvement of computer technology, many researchers have focused on numerical modeling to study CFRP machining. The numerical modeling of fiber-reinforced composites can be classified under two general approaches: (I) micromechanical approach, where the composite is modeled as a multi-phase material, and (II) macromechanical approach, where the composite part is modeled as an equivalent homogeneous material (EHM). The micromechanical approach has been used successfully to predict local defects (such as debonding) and cutting forces [3]. Nayak et al. [4] presented two micro- and macromechanical models and compared the predicted forces

Table 1 Mechanical and physical properties of CFRP unidirectional laminate (TC-09-U)

Mechanical properties	CFRP	Method/reference	Mechanical properties	CFRP	Method/reference
Longitudinal modulus, E_1 (GPa)	122.6	ASTM D3039	Longitudinal shear strength, S^L (MPa)	76.75	ASTM D5379
Transverse modulus, E_2 (GPa)	7.01	ASTM D3039	Transverse shear strength, S^T (MPa)	45.9	ASTM D5379
In-plane shear modulus, G_{12} (GPa)	12.669	ASTM D5379	Fracture energy-fiber tension (kJ/m^2)	91.6	[33]
Major Poisson's ratio ν_{12}	0.27		Fracture energy-fiber compression (kJ/m^2)	79.9	[33]
Longitudinal tensile strength, X^T (Mpa)	1388.0	ASTM D3039	Fracture energy-matrix cracking (kJ/m^2)	0.22	[33]
Longitudinal compressive strength, X^C (Mpa)	551.69	ASTM D6641	Fracture energy-matrix crushing (kJ/m^2)	1.1	[33]
Transverse tensile strength, Y^T (Mpa)	48.2	ASTM D3039	Specific gravity (g/cm^3)	1.552	ASTM D 792
Transverse compressive strength, Y^C (Mpa)	124.53	ASTM D6641			

of both with experimental results. They concluded that both models are able to accurately predict the principal cutting force, but the micromechanical models offer better estimations of thrust forces. They also indicated that the sub-surface damages and cutting forces increase with the fiber angle.

Despite the advantages presented by the micromechanical approach, it has some limitations. Micromodeling is more complex than macromodeling and requires very high calculation times and precise details regarding fibers, fiber-matrix arrangements, and their interfacial and physical properties. Therefore, many researchers have applied macromechanical approaches to model fiber-reinforced composite orthogonal cutting [3]. Lasri et al. [5] investigated the cutting of glass fiber-reinforced plastics (GFRP) using maximum stress, as well as the Hashin and Hoffman failure criteria. The principal cutting forces predicted with the Hashin criterion were closer to the experimentally measured data, but the predicted thrust forces for all failure criteria were much lower than the experiments'. Santiuste et al. [6] and Soldani et al. [2] confirmed the shortcoming of macromechanical modeling in predicting the thrust forces in orthogonal cutting of fiber-reinforced plastics. Mkaddem et al. [7, 8] developed a micro-macromodel to combine the advantages of both approaches. They considered the composite material as a homogeneous material, but the friction coefficient between the tool and the workpiece was assumed to be dependent on the fiber orientation. Their model successfully predicted the sub-surface damages and cutting and thrust forces with a lower mean error (6 % for cutting forces and 26 % for thrust forces) than did another macromechanical model presented by Nayak et al. (17 % for cutting forces and 44 % for thrust forces) [4]. Their modeling result demonstrated that the cutting forces increase with an increase of the fiber angle, while the thrust force increases with the fiber angle up to 45°, and then decreases to its minimum at 90°.

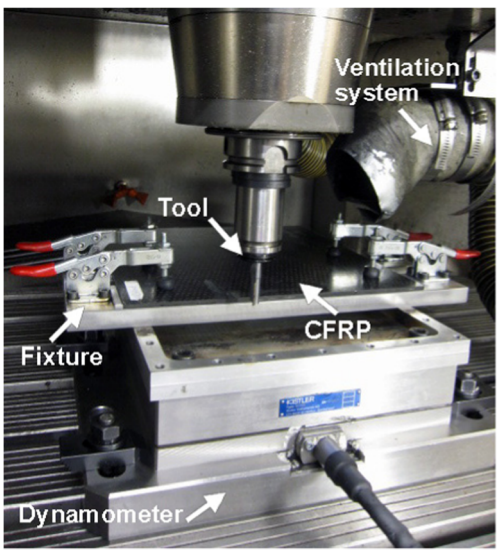

Fig. 1 Milling experiment set-up

To the authors' knowledge, although many models have been proposed for simulating the orthogonal cutting of CFRP, there is no numerical model simulating the machining of CFRP, such as the surface milling process. This work is therefore an attempt to present the first numerical model for CFRP milling. Despite the advantages of 3D modeling in comparison to 2D modeling, such as the ability to simulate out-of-plane failure (intralaminar and interlaminar (delamination) damages) [9, 10], it requires huge computation time. In addition, the authors' previous research showed that delamination is not the major concern during CFRP surface milling, compared to other machining processes such as drilling [11]. Thus, a two-dimensional finite element model was developed to study the cutting forces, chip formation, and machining damage occurring during CFRP milling. The composite material was modeled as an equivalent homogeneous material. An adaptive meshing approach was employed in the cutting zone, and the friction coefficient between the tool and workpiece was assumed dependent on fiber orientation.

In order to validate the developed model, milling experiments were performed and compared to the modeling results.

2 Experimental procedure

2.1 Composite materials

A high-performance carbon fiber epoxy unidirectional prepreg (P2053F-10) from Toray Inc., with a surface density of 100 g/m^2 and fiber volume content (V_f) of 60 %, was used to produce unidirectional CFRP laminate with a final average thickness of approximately 6.3 mm. The plates were then post-cured in an autoclave according to the cure cycle recommended by the supplier. The mechanical and physical properties of the material were needed for the modeling. Therefore, compression, shear, and tensile tests (according to ASTM D6641 [12], ASTM D5379 [13], and ASTM D3039 [14], respectively) were carried out in both the fiber and transverse directions of the unidirectional composite, and the specific gravity, also required as a physical property, was measured based on ASTM D-792 [15]. The material properties used in the model are summarized in Table 1.

2.2 Milling process

The milling experiments were carried out on a Huron K2X10 three-axis CNC machine with a maximum spindle speed of 28,000 rev/min (Fig. 1). A 3/8″ polycrystalline diamond (PCD) flat end mill (Fig. 2) was used for milling tests. Figure 2b shows the tool geometry, including the rake and relief angles that were measured using a Keyence VHC-]500F type digital microscope. An average tool edge radius of 5 μm was measured by an Olympus LEXT OLS4000 3D confocal laser microscope (Fig. 2d).

According to the results of the authors' previous research works [11, 16], a better surface quality can be achieved using a lower feed rate and a moderate cutting speed during CFRP surface milling. Therefore, in the present work, a moderate cutting speed of 250 m/min was used, while the feed rate was kept constant at 0.063 mm/rev (the lowest feed rate in the authors' previous research). The axial depth of cut was maintained constant at 0.5 mm for all milling tests. The milling

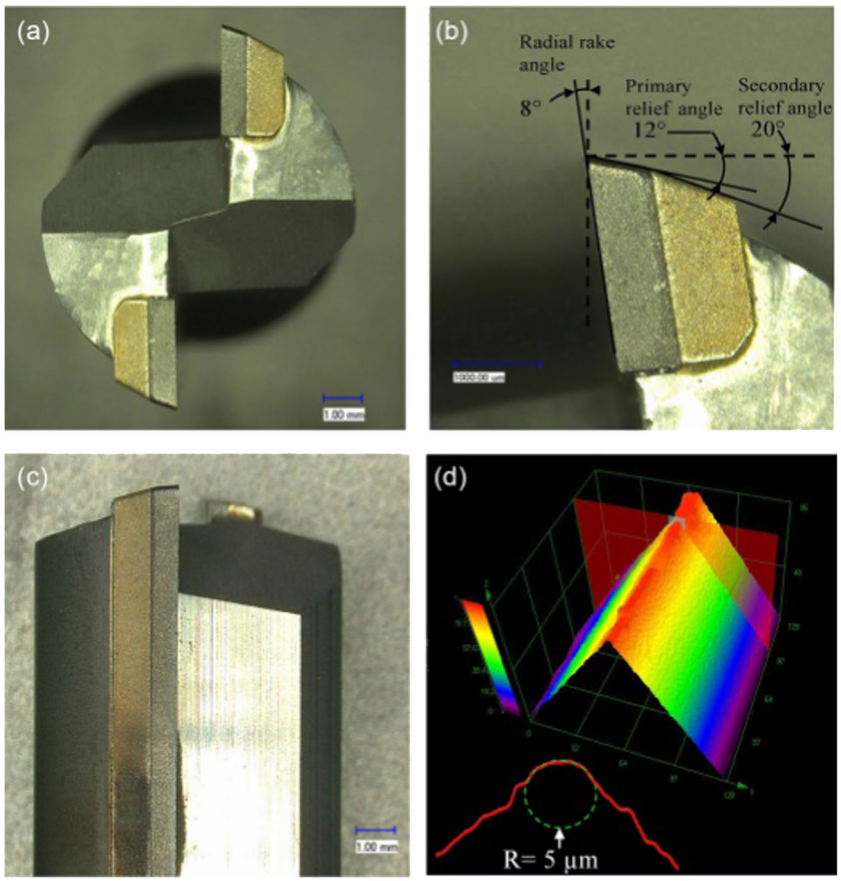

Fig. 2 Cutting tool geometry

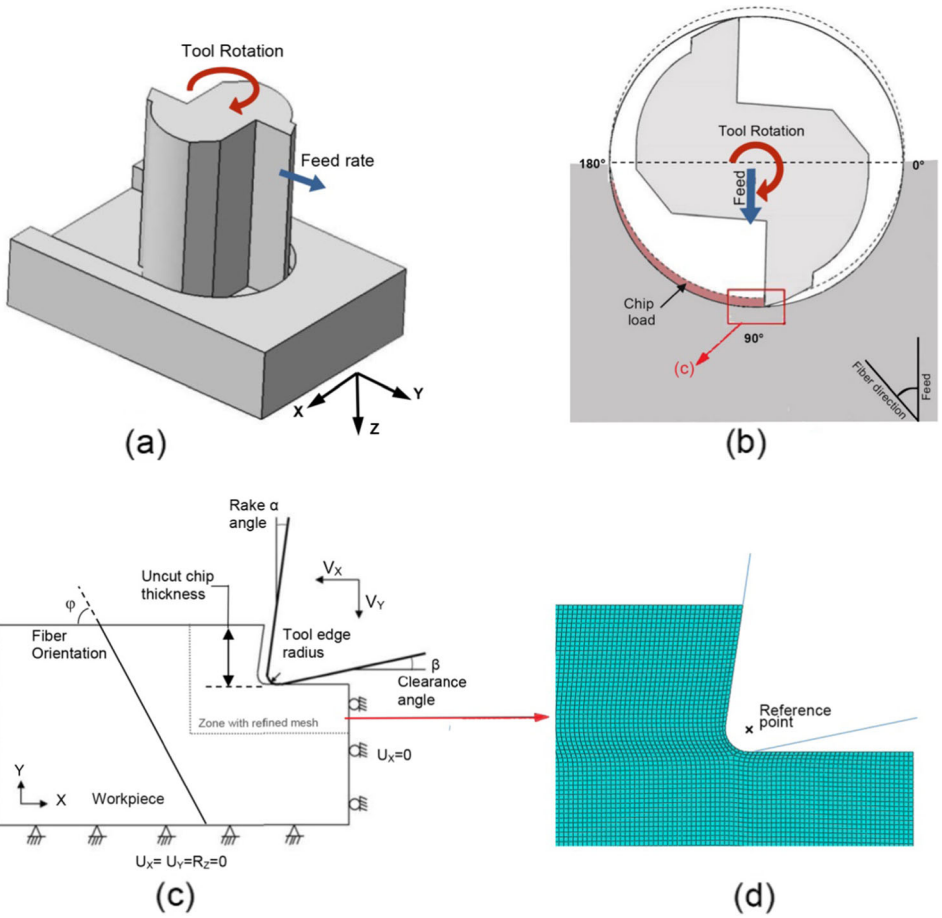

Fig. 3 Numerical modeling set-up

experiments were carried out with four different machining directions (defined in Fig. 3 by the angle between carbon fibers and the feed direction) of 0°, 45°, 90°, and 135°. The cutting forces during machining were measured using a Kistler 9255B(#3) three-axis dynamometer table connected to a Kistler-type 5010 charge amplifier (Fig. 1). A Mitutoyo SJ400 contact profilometer was used to measure the roughness of the machined surfaces. The surfaces and edges of the machined slots were also examined using a Hitachi S-3600N scanning electron microscopy (SEM).

3 Numerical modeling

3.1 Geometry, contact, meshing, and analysis

CFRP milling is a three-dimensional process and involves geometrically complex operations. Its modeling is thus very complex and requires huge computation time. A simplified two-dimensional orthogonal cutting model can describe the milling process very well, with a lower computation time than 3D modeling. During milling with a flat end mill, most of the cutting is performed using the periphery of the cutter. Figure 4

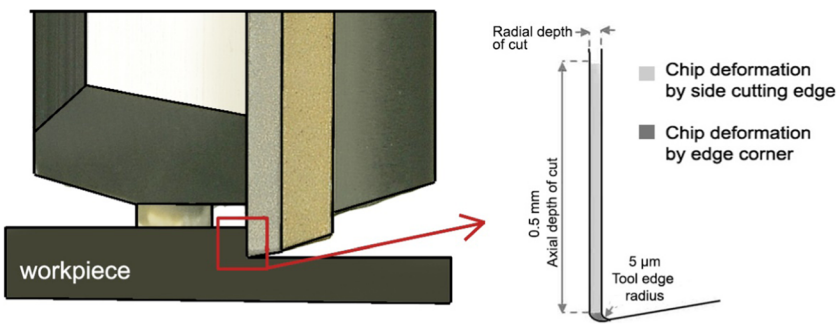

Fig. 4 The chip deformation by the tool side cutting edge and cutting edge corner

schematically shows that the chip deformation by the cutting edge corner is negligible as compared to that by the side cutting edge. As can be seen in Fig. 3b, the flat end milling process can then be assumed as the sum of a deck of 2D deformation process sections. To reduce the computation time, a simplified geometry of one cutting edge was modeled for a small portion (Fig. 3c) of the tool rotation and for different tool rotation angles: 30°, 45°, 60°, 90°, 120°, 135°, and 150°.

In the actual milling process, the cutting edge tip travels on a trochoidal path as a result of the feed rate and spindle rotation. However, the tool path can be assumed circular for small chip thickness values [17]. The conventional uncut chip thickness ($h_n(\theta)$) was calculated for different tool rotation angles (θ) by the following equation, based on the assumption of a circular tool path:

$$h_n(\theta) = f_z \sin\theta \quad (1)$$

where f_z represents the feed per tooth ($f_z = f/Z$, Z: number of teeth) [18].

The displacement of the workpiece bottom in the cutting and perpendicular directions, and the displacement of the workpiece extremities in the machining direction were restrained (Fig. 3c). The unidirectional CFRP was modeled as a homogeneous orthotropic material. A plane strain model is not appropriate for composite materials due to the out-of-plane material displacement observed during the cutting process [5]. A plane stress model was therefore considered, using continuum solid elements CPS4R, available in the commercial finite element code ABAQUS/Explicit version 6.12, and allowing linear interpolation, reduced integration, and automatic hourglass control. The milling tool was assumed to be a rigid body in order to save the computation time (the elastic modulus of polycrystalline diamond material is six times greater than that of CFRP in the fiber direction [19]). In many research works, the orthogonal cutting process is modeled based on quasi-static analysis, emphasizing the initial instant of the cutting process [5, 20, 21]. The low strain rate dependence of CFRP materials due to their brittle nature supports this assumption [5]. Thus, a quasi-static analysis was employed in the present study.

A reference point controlled the movement of the cutting tool (Fig. 3d), which was modeled with the geometry described in the previous section, with a rake angle of 8°, a clearance angle of 12°, and an edge radius of 5 μm. Wang and Zhang [22] found that there is a difference between the nominal and real depths of cut due to the bouncing back phenomenon. This phenomenon occurs when a certain part of the material below the tool is pushed down without cutting, partially producing an elastic springback after the tool passes through. Thus, in this model, the workpiece was configured with a round corner ahead of the cutting tool in order to take into account the bouncing back effect during cutting. As can be seen in Fig. 3c, the mesh of the workpiece was refined in the cutting zone surrounding the tool edge tip (mesh size of 10 μm, approximately equal to the fiber diameter). Arbitrary Lagrangian-Eulerian (ALE) adaptive meshing is a general formulation]that combines the features of pure Eulerian and pure Lagrangian analysis. This technique allows the mesh to move independently of the underlying material. Thus, it can control the element distortion and maintain a high-quality mesh, even in a process involving large material deformations, by allowing the mesh to move independently of the underlying material [23]. The ALE method was used in this research to reduce mesh distortion.

3.2 Contact modeling

The interaction between the work material and tool was modeled by using the surface-node surface contact available

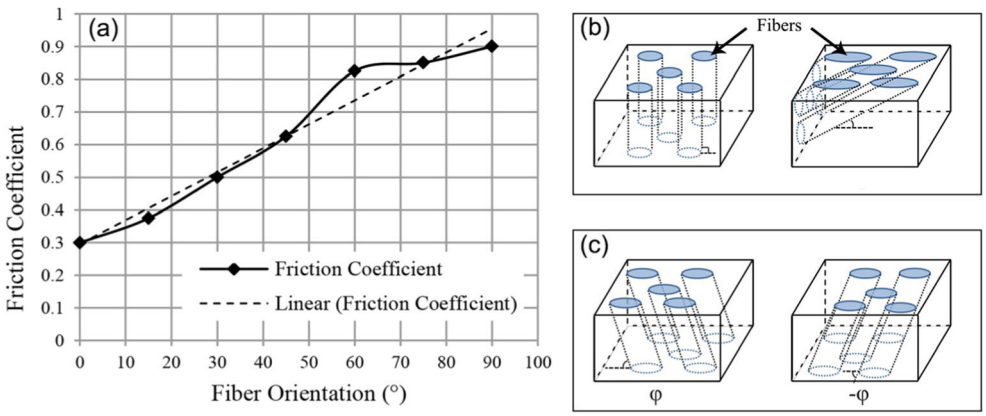

Fig. 5 **a** Variation of friction coefficient with respect to fiber orientation [4, 8], **b** effect of fiber orientation on fiber area fraction, and **c** fiber area fraction for φ and −φ fiber orientation

in ABAQUS/Explicit. The cutting tool was defined as the master object and the workpiece as the slave object. Friction is an important phenomenon that influences the accuracy of predicted cutting forces in machining simulation. In the present model, the friction between the workpiece and the cutting tool was described by Coulomb's friction law (Eq. 2), where the frictional stress (τ_n) on the tool is proportional to the normal stress (σ_n), with a constant friction coefficient (μ), such that

$$\tau_n = \mu\sigma_n \tag{2}$$

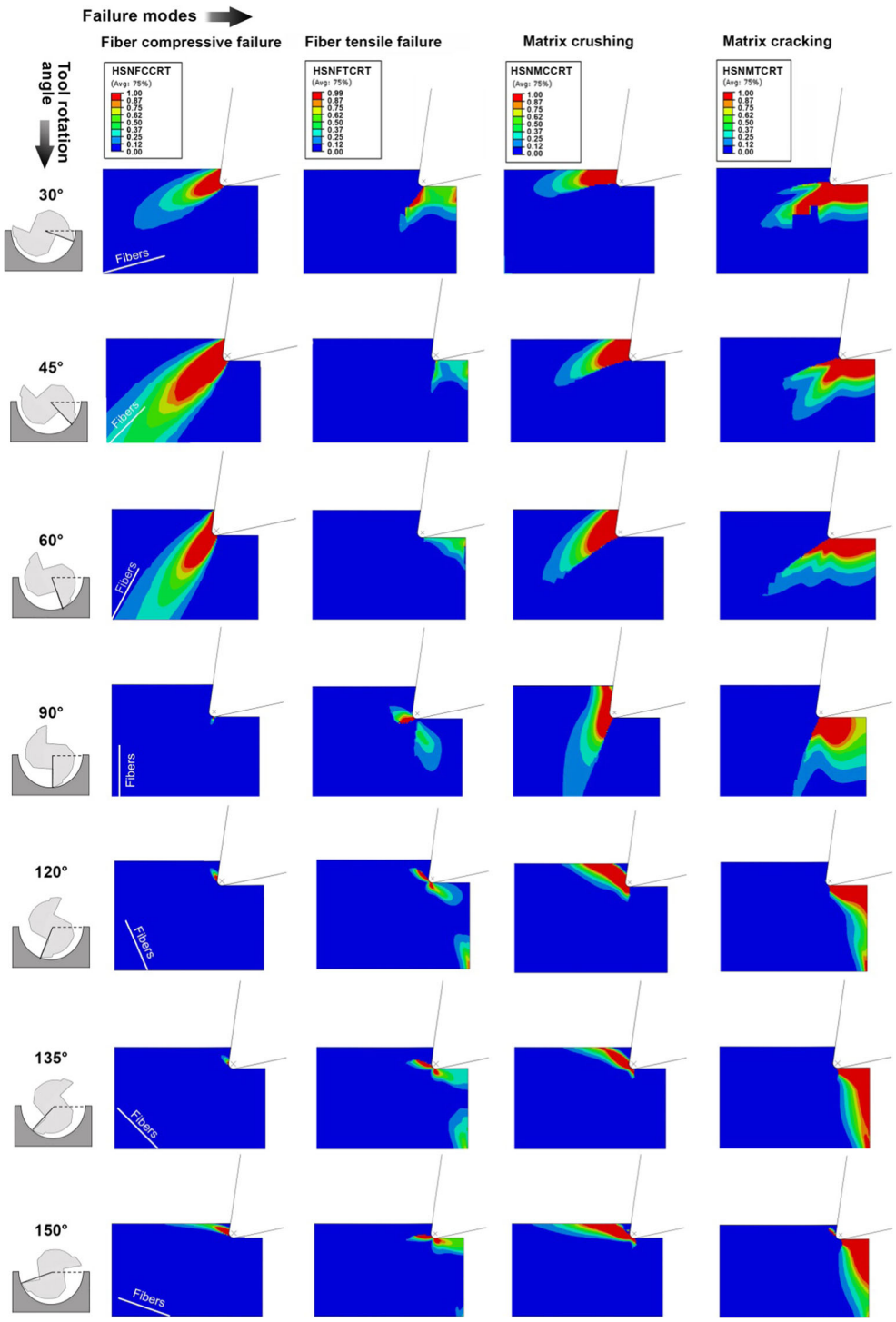

Fig. 6 Chip formation mechanism in milling of CFRP with a 0° feed rate orientation

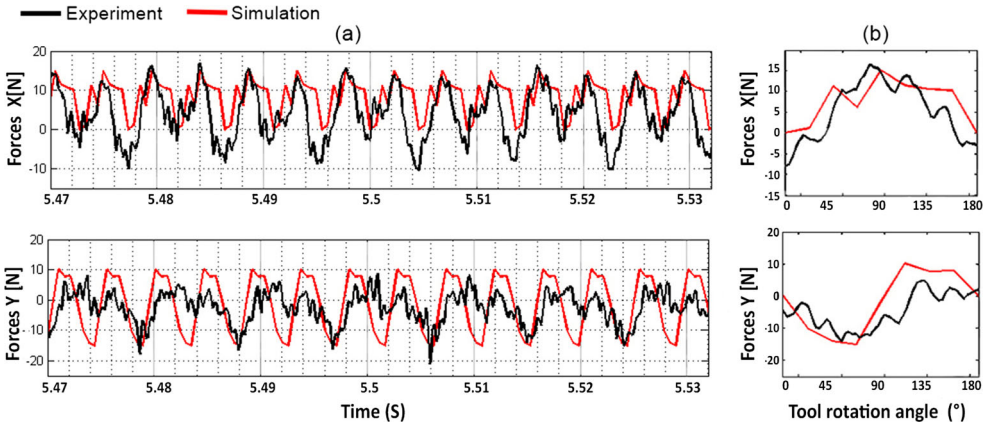

Fig. 7 Comparison between the experimental and simulated values of the cutting forces for a 0° machining direction, a 250 m/min cutting speed, a 0.063 mm/rev feed rate, and a 0.5-mm depth of cut

Many researchers assume a constant coefficient of friction for all fiber orientations, such as 0.3 [24–26], 0.4 [27], or 0.5 [5, 6]. Nayak and Bhatnagar [4] showed that the friction coefficient increased by increasing the fiber angle using pin-on-disk tests (Fig. 5a). The coefficient of friction is a function of the area fraction and coefficients of friction of the fiber and of the matrix phases in the composite [28]. The fiber orientation influences the fiber area fraction (as shown in Fig. 5b) and can therefore affect the composite friction coefficient. To enhance cutting force predictions, variable coefficients of friction (between 0.3 and 0.9) were determined for different fiber orientations, according to Nayak et al.'s research. Figure 5c shows that the fiber-reinforced composites with a negative and positive fiber orientation angle (φ and $-\varphi$) have the same fiber area fractions. Thus, the friction coefficient amounts in Fig. 5a were used for both positive and negative fiber orientation angles in modeling the tool/workpiece surfaces' contact.

4 Failure criteria

Lasri et al. [5] compared the maximum stress and Hashin and Hoffman failure criteria for the orthogonal cutting of FRP and concluded that cutting forces predicted using the Hashin failure criterion are closer to experimental results. Thus, Hashin's theory was used to predict damage and failure modes in this research. This failure criterion presents four failure modes, namely, fiber tensile failure, fiber compressive failure, matrix cracking, and matrix crushing modes, according to the following equations [29, 30]:

$$\text{Tensile fiber failure for } \sigma_{11}\geq 0: \quad \left(\sigma_{11}/X^T\right)^2+\alpha\left(\tau_{12}/S^L\right)^2\leq 1 \tag{3}$$

$$\text{Fiber compression } (\sigma_{11}<0): \quad \left(\sigma_{11}/X^C\right)^2\leq 1 \tag{4}$$

$$\text{Matrix cracking } (\sigma_{22}>0): \quad \left(\sigma_{22}/Y^T\right)^2+\left(\tau_{12}/S^L\right)^2\leq 1 \tag{5}$$

$$\text{Matrix crushing } (\sigma_{22}>0): \quad \left(\sigma_{22}/2S^T\right)^2+\left[\left(Y^C/2S^T\right)^2-1\right]\left(\sigma_{22}/Y^C\right)+\left(\tau_{12}/S^L\right)^2\leq 1 \tag{6}$$

where σ_{11}, σ_{22}, and σ_{12} are the normal stresses in the fiber and transverse directions and the in-plane shear stress, respectively. All other variables are listed in Table 1. The onset of damage was predicted using Hashin's failure criterion, and material degradation was modeled by reducing the material stiffness to 0. Reducing the stiffness to 0 occurs gradually in the modeling process by controlling damage variables, varying between 0 for the undamaged state to 1 for the fully damaged state. The evolution law of the damage variable is based on the fracture energy dissipated during the damage process [31].

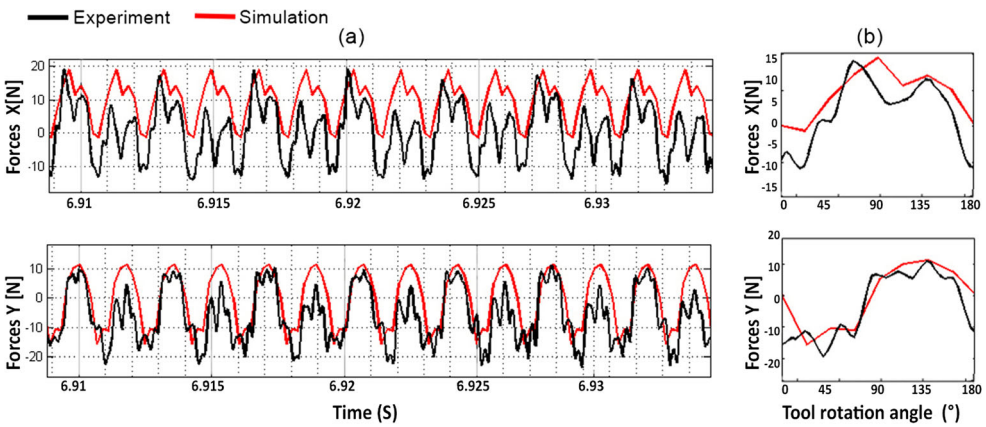

Fig. 8 Comparison between the experimental and simulated values of the cutting forces with a 90° machining direction, 250 m/min cutting speed, 0.063 mm/rev feed rate, and 0.5-mm depth of cut

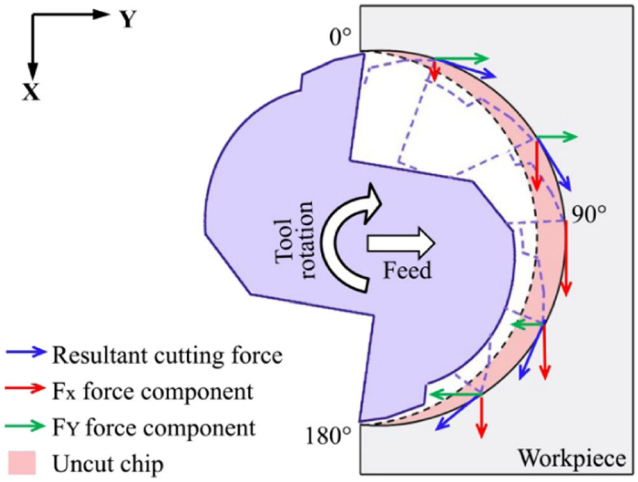

Fig. 9 Resultant cutting forces and the force components in X and Y directions for different tool rotation angles

The fracture energies used in the model for the different failure modes are presented in Table 1.

5 Results and discussion

5.1 Chip formation

In the model, the tool moves towards the workpiece material until a complete chip is formed after reaching material failure on the free surface ahead of the cutting tool. Figure 6 shows the chip formation process for different tool rotation angles in CFRP milling, with a machining direction of 0°. The horizontal and vertical axes (on the top and left sides of the figure) represent the failure modes and tool rotation angle, respectively. At low tool rotation angles (30°, 45°, and 60°), the fiber compressive failure and matrix crushing progressed in the fiber direction until completion of the chip formation. For higher tool rotation angles (90° and more), while the cutting tool progresses in the workpiece, a stressed zone is formed ahead of the tool edge, and matrix crushing damage is extended in the fiber direction until chip formation. The matrix cracking damage mode is illustrated in the last column of Fig. 6. It can be seen that matrix cracking failure affected a relatively large zone of uncut material below the tool for all tool rotation angles. The second column of Fig. 6 shows the fiber tensile failure mode for all tool rotation angles. The effect of this failure mode was almost negligible on the limited area ahead of the tool tip.

Comparing the fiber compression damage mode of all tool rotation angles in Fig. 6 (the first column) demonstrates that compression failure occurs in the direction of fibers. For 45° and 60° tool rotations, a large zone of uncut material is affected by this failure mode. Similarly, Santiuste et al. [6] concluded that the matrix failure modes (matrix crushing and cracking damages) control the chip formation in CFRP orthogonal cutting. Their results also showed that the effect of fiber failure modes is almost negligible in the chip formation mechanism, while the findings of the present research show that the effect of fiber compressive failure is significant for lower tool rotation angles.

The materials' behavior under load can generally be classified as ductile or brittle, based on their ability to undergo plastic deformation before fracture [32]. Santiuste et al. [6] found, from finite element analysis results, that glass fiber-reinforced plastics behave like ductile materials by showing a progressive damage process, while CFRPs are brittle materials showing little or no progression of damage. These results are supported by the actual modeling results demonstrating that CFRPs undergo catastrophic failure with negligible plastic deformation.

5.2 Cutting forces

Cutting forces in the X and Y directions are calculated in the model from the reaction exerted by the workpiece material on the tool reference point (Fig. 3d). The cutting forces obtained from the 0° and 90° milling directions are shown in Figs. 7 and 8, respectively. These figures show a good agreement between the experimental and predicted values of the cutting forces. The left images (Figs. 7a and 8a) show the cutting forces in the

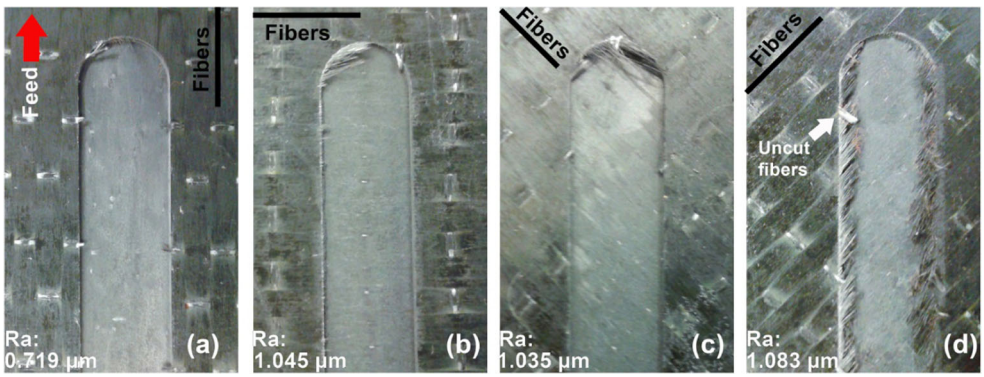

Fig. 10 CFRP machined surface for different machining directions of **a** 0°, **b** 45°, **c** 90°, and **d** 135°, 250 m/min cutting speed, 0.063 mm/rev feed rate, and 0.5-mm depth of cut

time domain for seven complete rotations of the tool (the two-flute tool generating 14 peaks in the graph), and the right images (Figs. 7b and 8b) show the cutting forces of one tooth for a 180° rotation of the tool. Each peak of the force profile in Figs. 7a and 8a thus represents the passage of one tooth. It is clearly shown that the force profiles for the two teeth of the tool are not completely similar. The small difference seen can be explained by the tool run-out during the milling process. Tool run-out affects the cutting forces profile in conventional milling operations by affecting the feed per tooth of each tooth [18].

By comparing the cutting forces in Figs. 7b and 8b, it can be observed that those forces do not have similar profiles and amplitudes for different machining directions. It thus seems that fiber orientation has a significant effect on the cutting force profiles during machining of unidirectional CFRP. This can be explained by the anisotropic character of unidirectional fiber-reinforced plastic materials.

Figure 9 shows the resultant cutting forces and force components in the X and Y directions for different tool rotation angles. As can be seen in this figure, the cutting force components in the X direction (F_X, red arrows) are always in the positive direction of the X-axis. The model developed also predicted the positive amount of the cutting forces in the X direction (red lines in Figs. 7a and 8a) for all tool rotation angles, while a negative F_X was experimentally measured for some edge passages (black lines in Figs. 7a and 8a) in the 180° tool rotation, where the chip thickness is theoretically equal to 0. This difference between the experimental and modeling results can be explained by the tool run-out that affects the thickness and shape of the uncut chip area.

5.3 Surface integrity

Figure 10 shows the CFRP machined surface for different machining directions (0°, 45°, 90°, and 135°). The best surface quality in terms of surface roughness (R_a—arithmetic average height) and lowest damage was achieved in the 0° machining direction. As shown in Fig. 10d, many uncut fibers are observed in milling at 135°, fibers that protrude from the machined edges, resulting in a poor edge quality.

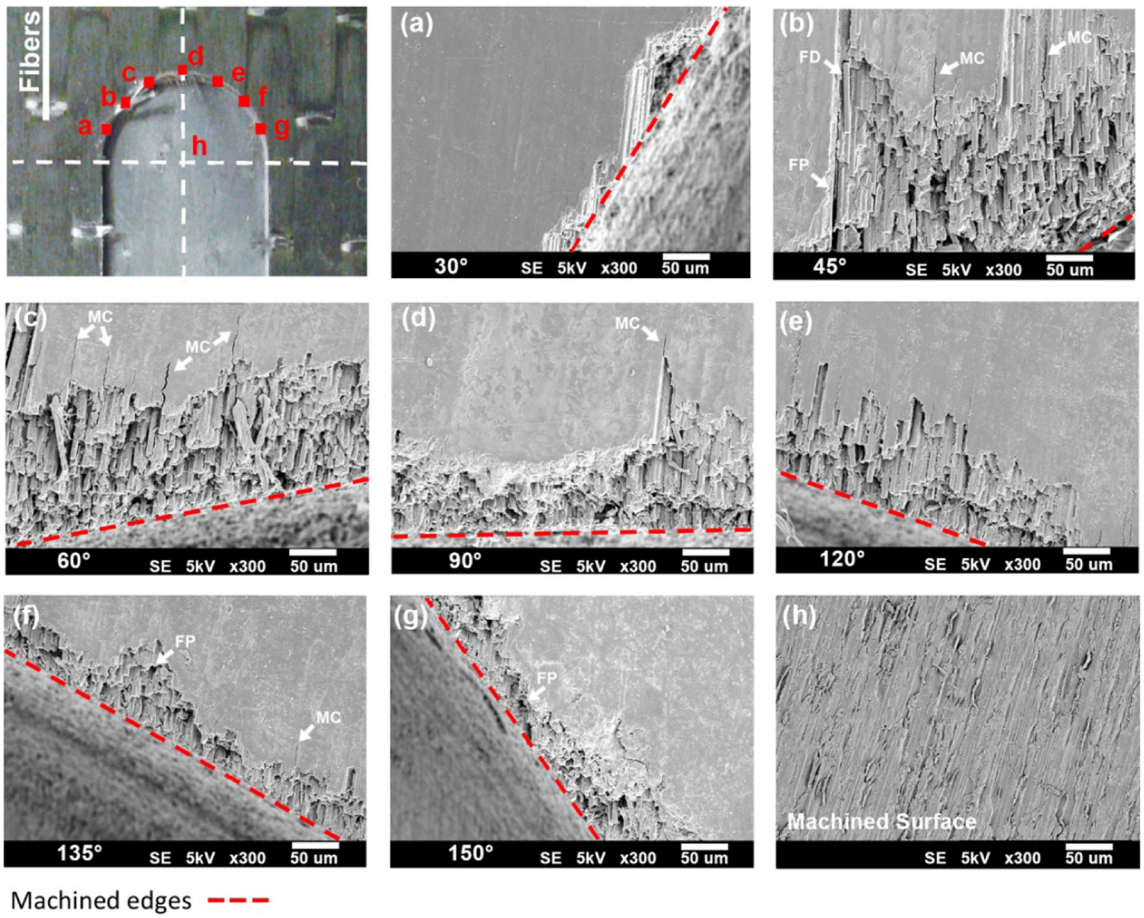

Fig. 11 Machining damage at different tool rotation angles: fiber pullout (*FP*), fiber/matrix de-cohesion (*FD*), matrix cracking (*MC*)

Figure 11 illustrates the SEM photographs of the machined surface and edges for different tool rotation angles and for the 0° machining direction. As can be seen, the larger damaged zones on the machined edges are observed at tool rotation angles of 45° and 60° (Fig. 11b, c), compared to other tool rotation angles (Fig. 11a, d, e). This is in agreement with Fig. 6, where the modeling results show that the compressive damage failure mode affects a large zone of uncut materials for tool rotation angles of 45° and 60°. As described in the modeling results, matrix cracking failure affects a relatively large zone around the cutting area. This modeling prediction is confirmed by the presence of deep matrix cracking damage in SEM images. A SEM image of the machined surface is shown in Fig. 11h. As can be seen, a good surface quality was produced with the cutting condition used in this research (250 m/min cutting speed, 0.063 mm/rev feed rate, 0.5-mm depth of cut).

6 Conclusion

In this work, the surface milling of unidirectional carbon fiber-reinforced laminates was studied by comparing finite element analysis results with experimental results. The chip formation mechanism, machining damage, and cutting forces were investigated with the proposed finite element model. Based on the results, the following conclusions are drawn:

- The developed 2D finite element model provided a better understanding of the CFRP surface milling process. The model was validated by comparing its results with experimentally measured forces and SEM images of the machined surface. The model was able to predict the cutting forces and machining damages, which is in good agreement with experiments.
- The cutting forces do not have similar profiles for different machining directions (angle between the carbon fibers and feed direction), meaning that the cutting force profile depends considerably on the fiber orientation.
- At low tool rotation angles (30°–60°), the fiber compressive failure and matrix crushing progressed in the fiber direction until completion of the chip formation, while at higher tool rotation angles (90° and more), the chip was formed in matrix crushing mode.
- The extension of machining damage significantly depends on the fiber orientation. During milling in a 0° machining direction, for all tool rotation angles, the compressive damage in uncut materials extended in the direction of fibers. For 45° and 60° tool rotations, this failure mode affects a large zone of uncut materials, as was confirmed by micrographic images. The matrix cracking failure also affected a relatively large zone of uncut material below the tool for all tool rotation angles.
- The numerical predictions of machining damage around the cutting area, due to fiber compressive damage and matrix cracking, were confirmed by SEM images of the edges and surface of the machined zone.

Acknowledgments This study was funded by the Consortium for Research and Innovation in Aerospace in Quebec (CRIAQ) and the Natural Sciences and Engineering Research Council of Canada (NSERC).

References

1. Davim JP (2015) Machinability of fibre-reinforced plastics, vol 4. Walter de Gruyter GmbH & Co KG, Berlin
2. Soldani X, Santiuste C, Muñoz-Sánchez A, Miguélez M (2011) Influence of tool geometry and numerical parameters when modeling orthogonal cutting of LFRP composites. Compos A: Appl Sci Manuf 42(9):1205–16
3. Dandekar CR, Shin YC (2012) Modeling of machining of composite materials: a review. Int J Mach Tool Manuf 57:102–21
4. Nayak D, Bhatnagar N, Mahajan P (2005) Machining studies of UD-FRP composites part 2: finite element analysis. Mach Sci Technol 9(4):503–28
5. Lasri L, Nouari M, El Mansori M (2009) Modelling of chip separation in machining unidirectional FRP composites by stiffness degradation concept. Compos Sci Technol 69(5):684–92
6. Santiuste C, Soldani X, Miguélez MH (2010) Machining FEM model of long fiber composites for aeronautical components. Compos Struct 92(3):691–8
7. Mkaddem A, Demirci I, El Mansori M (2008) A micro–macro combined approach using FEM for modelling of machining of FRP composites: cutting forces analysis. Compos Sci Technol 68 (15):3123–7
8. Mkaddem A, El Mansori M (2009) Finite element analysis when machining UGF-reinforced PMCs plates: chip formation, crack propagation and induced-damage. Mater Des 30(8):3295–302
9. Santiuste C, Olmedo A, Soldani X, Miguélez H (2012) Delamination prediction in orthogonal machining of carbon long fiber-reinforced polymer composites. J Reinf Plast Compos 31(13): 875–85
10. Isbilir O, Ghassemieh E (2013) Three-dimensional numerical modelling of drilling of carbon fiber-reinforced plastic composites. Journal of Composite Materials:0021998313484947
11. Ghafarizadeh S, Lebrun G, Chatelain J-F (2015) Experimental investigation of the cutting temperature and surface quality during milling of unidirectional carbon fiber reinforced plastic. Journal of Composite Materials:0021998315587131
12. ASTM (2009) D6641/D6641M-09: Standard test method for compressive properties of polymer matrix composite materials using a combined loading compression (CLC) test fixture. West Conshohocken, PA
13. ASTM (2012) D5379/D5379M: Standard test method for shear properties of composite materials by the V-notched beam method. West Conshohocken, PA
14. ASTM (2014) D3039/D3039M: Standard test method for tensile properties of polymer matrix composite materials. West Conshohocken, PA
15. ASTM (2008) D 792–08. Standard test methods for density and specific gravity (relative density) of plastics by displacement. West Conshohocken, PA

16. Ghafarizadeh S, Chatelain J-F, Lebrun G (2014) Effect of cutting tool lead angle on machining forces and surface finish of CFRP laminates. Science and Engineering of Composite Materials
17. Özel T, Altan T (2000) Process simulation using finite element method —prediction of cutting forces, tool stresses and temperatures in high-speed flat end milling. Int J Mach Tool Manuf 40(5):713–38
18. Li C, Lai X, Li H, Ni J (2007) Modeling of three-dimensional cutting forces in micro-end-milling. J Micromech Microeng 17 (4):671
19. Ramulu M, Faridnia M, Garbini J, Jorgensen J (1991) Machining of graphite/epoxy composite materials with polycrystalline diamond (PCD) tools. J Eng Mater Technol 113(4):430–6
20. Arola D, Ramulu M (1997) Orthogonal cutting of fiber-reinforced composites: a finite element analysis. Int J Mech Sci 39(5):597–613
21. Ramesh M, Seetharamu K, Ganesan N, Sivakumar M (1998) Analysis of machining of FRPs using FEM. Int J Mach Tool Manuf 38(12):1531–49
22. Wang X, Zhang L (2003) An experimental investigation into the orthogonal cutting of unidirectional fibre reinforced plastics. Int J Mach Tool Manuf 43(10):1015–22
23. Hibbitt D, Karlsson B, Sorensen P (2012) Abaqus 6.12 documentation and user manual. Dassault Systèmes Simulia Corp.
24. Rao GVG, Mahajan P, Bhatnagar N (2007) Machining of UD-GFRP composites chip formation mechanism. Compos Sci Technol 67(11):2271–81
25. Rao GVG, Mahajan P, Bhatnagar N (2007) Micro-mechanical modeling of machining of FRP composites—cutting force analysis. Compos Sci Technol 67(3):579–93
26. Rentsch R, Pecat O, Brinksmeier E (2011) Macro and micro process modeling of the cutting of carbon fiber reinforced plastics using FEM. Procedia engineering 10:1823–8
27. Arola D, Sultan M, Ramulu M (2002) Finite element modeling of edge trimming fiber reinforced plastics. J Manuf Sci Eng 124(1): 32–41
28. Schön J (2004) Coefficient of friction and wear of a carbon fiber epoxy matrix composite. Wear 257(3):395–407
29. Hashin Z (1980) Failure criteria for unidirectional fiber composites. J Appl Mech 47(2):329–34
30. Hashin Z, Rotem A (1973) A fatigue failure criterion for fiber reinforced materials. J Compos Mater 7(4):448–64
31. Lapczyk I, Hurtado JA (2007) Progressive damage modeling in fiber-reinforced materials. Compos A: Appl Sci Manuf 38(11): 2333–41
32. Dieter GE, Bacon D (1986) Mechanical metallurgy, vol 3. McGraw-Hill New York
33. Shi Y, Swait T, Soutis C (2012) Modelling damage evolution in composite laminates subjected to low velocity impact. Compos Struct 94(9):2902–13